Aqueous Ring-Opening Polymerization-Induced Self-Assembly (ROPISA) of N-carboxyanhydrides

Chloé Grazon, Pedro Salas-Ambrosio, Emmanuel Ibarboure, Alix Buol, Elisabeth Garanger, Mark W. Grinstaff, Sébastien Lecommandoux, Colin Bonduelle

Author manuscript of article published in *Angew. Chem. Int. Ed. 2019*

Aqueous Ring-Opening Polymerization-Induced Self-Assembly (ROPISA) of *N*-carboxyanhydrides

Chloé Grazon, Pedro Salas-Ambrosio, Emmanuel Ibarboure, Alix Buol, Elisabeth Garanger, Mark W. Grinstaff, Sébastien Lecommandoux,* Colin Bonduelle*

Received September 19 2019, accepted online October 24 2019

DOI 10.1002/anie.201912028

Dr C. Grazon, P. Salas-Ambrosio, E. Ibarboure, A. Buol, Dr E. Garanger, Prof. S. Lecommandoux, Dr C. Bonduelle
CNRS, Bordeaux INP, LCPO, UMR 5629, Univ. Bordeaux, F-33600, Pessac, France
E-mail: colin.bonduelle@enscbp.fr, lecommandoux@enscbp.fr

Dr C. Grazon, Prof. M. W. Grinstaff
Departments of Chemistry and Biomedical Engineering, Boston University, Boston, MA, USA

Abstract: Reported here is the first aqueous ring-opening polymerization (ROP) of *N*-carboxyanhydrides (NCA) using α-amino-poly(ethylene oxide) macroinitiator to protect NCA monomers from hydrolysis through spontaneous *in situ* self-assembly (ISA). This ROPISA process affords well-defined amphiphilic diblock copolymers that simultaneously form original needle-like nano-objects.

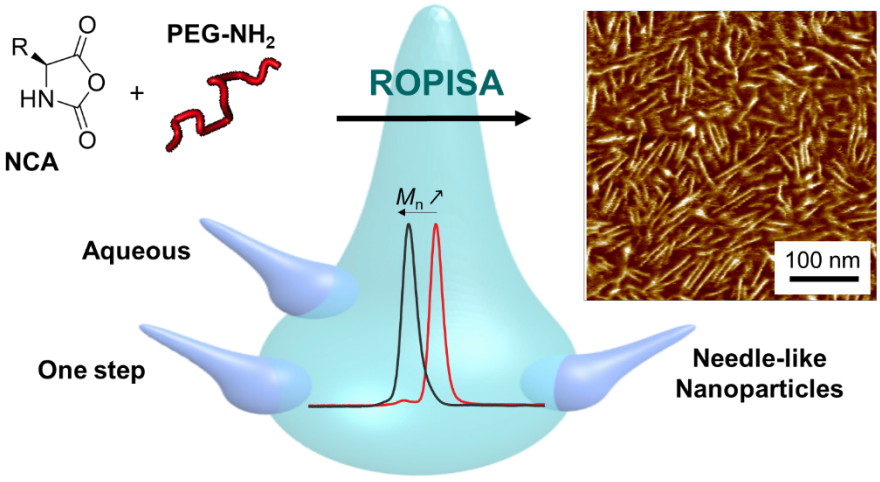

C. Grazon, P. Salas-Ambrosio, E. Ibarboure, A. Buol, E. Garanger, M.W. Grinstaff, S. Lecommandoux, C. Bonduelle, Angewandte Chemie International Edition 2019. DOI 10.1002/anie.201912028

Self-assembly of amphiphilic polymers is a promising strategy to design advanced nanomaterials with unique properties.[1] Among those polymers, naturally produced or chemically synthesized polypeptides are an emerging class of biomaterials.[2] In nanomedicine, the ability to precisely design amphiphilic polypeptides to suit a specific function is a significant advantage: amphiphilic polypeptides offer a unique approach to guide nanoscale structure formation through intermolecular and/or intramolecular interactions.[3] As a result, amphiphilic polypeptides are extensively used as nanosized drug carriers in pharmaceutical applications.[4] So far, the most economical and efficient process to prepare polypeptides is a one-step process based on the ring-opening polymerization of *N*-carboxyanhydride monomers (ROP of NCA, Scheme 1A).[5] This controlled polymerization uses simple reagents and allows the preparation of polymers in both good yields and large quantities. However, NCA polymerizations suffer from significant limitations including tedious monomer purification steps,[6] significant sensitivity to moisture,[7] and processing in toxic organics solvents such as DMF that need to be subsequently removed.[8]

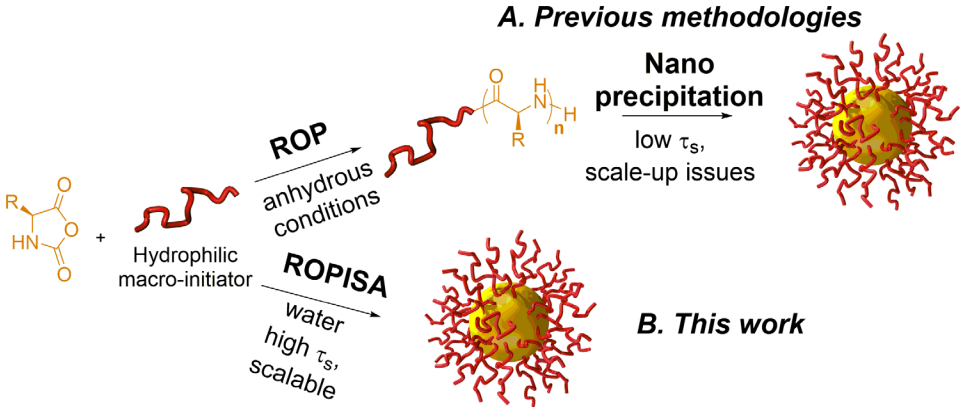

Scheme 1. Methods for the preparation of core-shell nanoparticles stabilized by amphiphilic block polypeptides. A. Block copolymer synthesis *via* ROP followed by a nanoprecipitation step. B. One-step approach by Ring-Opening Polymerization-Induced Self-Assembly (ROPISA).

To improve the synthesis conditions, recent efforts are focused on promoting the polymerization rate without the use of a catalyst, exploring new more reactive initiators, and using specific processes including emulsion polymerization approaches.[9] For example, Wooley *et al*. demonstrated that removal of CO_2 *via* a N_2 flow during polymerization of γ-benzyl-*L*-glutamate *N*-carboxyanhydrides (BLG-NCA) produced polypeptides with predictable molar masses and narrow distributions.[10] Similar advances are achieved using ultrafast new ROP initiators, such as triethylaminetriamine (TREN)[11] or LiHMDS.[12] The latter initiator is particularly suitable as the polymerization is performed in an open-air vessel despite NCA moisture sensitivity.[12] Finally, Cheng *et al.* reported the *in situ* purification of NCA during ROP when the polymerization was conducted in a CH_2Cl_2 / water emulsion.[13]

Unfortunately, the preparation of nanoassemblies from amphiphilic polypeptides requires a second step of nanoprecipitation (Scheme 1A), which entails the addition of a non-solvent for the hydrophobic segment to a copolymer solution in a common solvent for both blocks.[14] This nanoprecipitation step is typically performed from toxic organic solvents, under relatively diluted conditions (<1 wt%) and is sensitive to scale issues, overall hampering eventual regulatory

C. Grazon, P. Salas-Ambrosio, E. Ibarboure, A. Buol, E. Garanger, M.W. Grinstaff, S. Lecommandoux, C. Bonduelle, Angewandte Chemie International Edition 2019. DOI 10.1002/anie.201912028

approval.[15] The above mentioned emulsion polymerization approach is a potential scalable methodology to form nanosized platform for therapeutic cargo.[16] In this context, polymerization-induced self-assembly (PISA) is a facile, rapid, and robust approach for accessing amphiphilic copolymers with the added benefit of simultaneously obtaining polymeric nanoparticles.[17] PISA involves the *in situ* growth of a living amphiphilic polymer chain during its self-assembly into nanostructures. To date, PISA is accomplished predominantly using controlled radical polymerization processes (such as RAFT) in dispersion or emulsion.[18] Literature examples of PISA utilizing ring-opening polymerization are scarce.[19] Adaptation of aqueous PISA to NCA compounds is unprecedented and not obvious given the well documented sensitivity of NCA monomers to hydrolysis.[20]

Specifically, we report the aqueous Ring-Opening Polymerization Induced Self-Assembly (ROPISA, scheme 1B) of NCA monomers with the hydrophilic macromolecular initiator α-amino-poly(ethylene oxide). Ring-opening polymerization affords well-defined amphiphilic polypeptides in high yield and narrow dispersity as well as their related nanoparticles, as characterized by DLS, AFM and cryo-TEM. Usually, water is strictly removed from conventional ROP medium, as it otherwise leads to water-induced NCA hydrolysis and uncontrolled polymerization. In order to obtain selective NCA polymerizations in aqueous solutions, we envision two requirements to be met. First, the amine-related nucleophilic attack must occur at a comparatively faster rate than hydrolysis. [21] Second, micelles from short diblock of PEG-*b*-PBLG (early stage of the polymerization) must protect the remaining NCA monomers. With regards to the former, NCA aminolysis is pH dependent and, at certain pH conditions, aminolysis is faster than hydrolysis.[21a,21b] With regards to the later, a polymer which facilitates micellar formation – such as a diblock based on poly(ethylene glycol) and hydrophobic segment - and acts as a macroinitiator is a prime candidate for investigation.

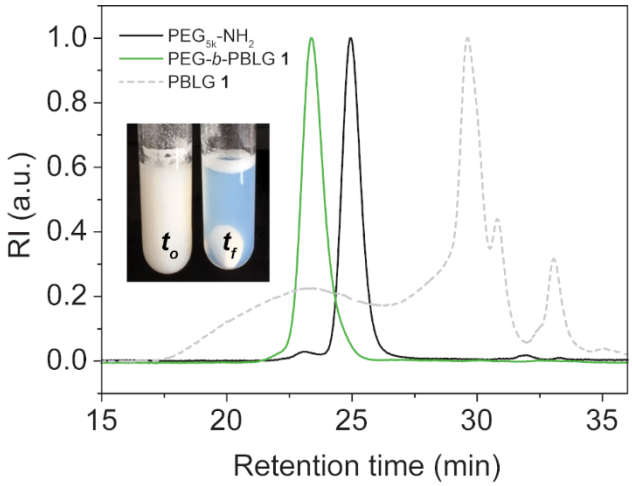

Figure 1. Size exclusion chromatograms in DMF (1mg/mL LiBr, RI detection) of PEG-*b*-PBLG 1 (DP = 19, τ_s = 7%), control PBLG 1 (only BLG in MQ water) and the reference PEG_{5k}-NH_2. Insert show pictures of the dispersion polymerization just after adding BLG powder (t_0) and at the end of the polymerization (t_f).

C. Grazon, P. Salas-Ambrosio, E. Ibarboure, A. Buol, E. Garanger, M.W. Grinstaff, S. Lecommandoux, C. Bonduelle, Angewandte Chemie International Edition 2019. DOI 10.1002/anie.201912028

Thus, we identified a sodium bicarbonate aqueous solution (pH= 8.5, 50 mM) as the buffer and α-amino-poly(ethylene glycol) (PEG_{5k}-NH_2 = 5 kg/mol, M_n = 4.9 kDa, $Đ$ = 1.08) (Scheme SI 1) as the initiator for ROP of γ-benzyl-*L*-glutamate *N*-carboxyanhydrides (BLG-NCA). In a typical experiment, we added 300 mg of PEG_{5k}-NH_2 in 8 mL of aqueous $NaHCO_3$ buffer to 300 mg of BLG-NCA powder. At 4°C and upon extensive stirring, this procedure affords opalescent solutions with a solids content (τ_s) of 7% (Fig 1). The nanoparticles are made of well-defined PEG-*b*-PBLG diblock copolymers with very narrow dispersity (PEG-*b*-PBLG **1**, M_n = 9.4 kDa, $Đ$ = 1.10, Fig 1, Fig SI 1 and 7, Table SI 1) in good yield (≈85%).

The experimental molar mass (M_n) is in good agreement with the theoretical one. Under these experimental condition ($[M]_0$ = 0.14 M), the apparent kinetic rate for ROPISA initiated by an α-amino-poly(ethylene glycol) is 0.14 $M^{-1}.s^{-1}$, as calculated from FTIR analyses (Fig SI 11). This kinetic rate is in the range of previously measured ROP of BLG-NCA enhanced by proximity-induced cooperative polymerization.[22] To further study the kinetics of this aqueous ROP process, we followed the polymerization propagation using a quenching method (see *Mat&Meth* SI). The kinetics analysis confirmed a linear evolution of molar mass with the BLG-NCA conversion, and that after 180 min, the degree of conversion is greater than 90% (Fig 2, Fig SI 12).

Upon full NCA conversion, we observed bluish solutions typical of nanoscale colloids (Fig 1, Table 1). After dilution to 1 mg/mL, DLS analysis revealed a monodisperse ($\sigma < 0.1$) nanoparticle distribution with a z-average diameter of about 80 nm. Interestingly, adding a subsequent feed of BLG-NCA to the colloidal solution resulted in chain extension (PEG-*b*-PBLG **6**, M_n = 11.3 kDa, $Đ$ = 1.16, Fig SI 4 and 8).

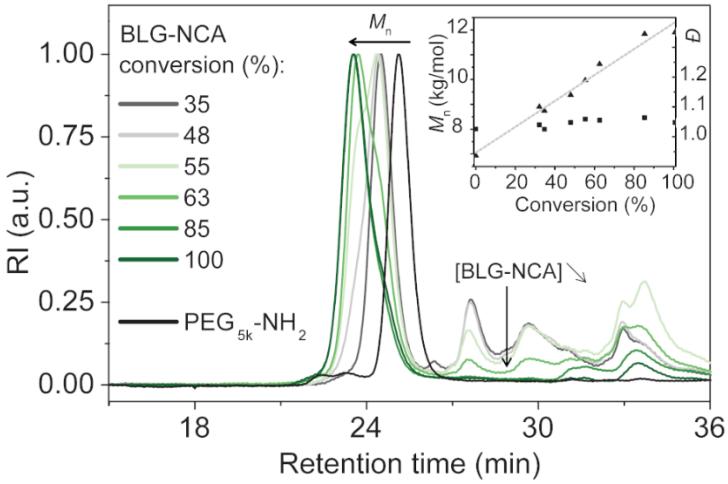

Figure 2. Kinetics study of PEG-*b*-PBLG **1** formation during the ROPISA followed by SEC in DMF (+ 1mg/mL of LiBr). Chromatograms at different time of reaction. Insert: Evolution of M_n ▲and $Đ$ ■ (determined by SEC in DMF, PS calibration) with BLG-NCA conversion (determined by ^1H NMR in $CDCl_3$).

C. Grazon, P. Salas-Ambrosio, E. Ibarboure, A. Buol, E. Garanger, M.W. Grinstaff, S. Lecommandoux, C. Bonduelle, Angewandte Chemie International Edition 2019. DOI 10.1002/anie.201912028

As before, the molar mass determined by ^{1}H NMR was in good agreement with the targeted degree of polymerization ([M]/[I] = 35) and the polymerization occurs without significant hydrolysis. The macromolecular hydrophilic initiator is important: first, in our procedure the PEG_{5k}-NH_2 concentrations are close to its CMC, and second, polymerization with ethanolamine or PEG_{5k}-OH initiators under similar conditions afford a complex mixture of aggregated oligomers (PBLG **2** and PBLG **3,** Fig SI 2 and Table SI 1). Collectively, these results support the idea that in the presence of the hydrophilic macroinitiator, NCA monomers hydrolysis could be avoided due to a rapid or a combined polymerization/self-assembly process. These observations could be consistent with the "classical" PISA mechanism where high monomer conversion occurs within short reaction times compared to conventional solution polymerization.[23]

Table 1. Diblock copolymers obtained by ROPISA at different solids content.

Exp	τ_s (%) [a]	M_n (kg/mol) [b]	$Đ$ [b]	D_h (nm) (σ) [c]
PEG-b-PBLG 2	4	8.92	1.08	83 (0.1)
PEG-b-PBLG 1	7	9.36	1.10	79 (0.08)
PEG-b-PBLG 3	10	9.94	1.09	80 (0.11)
PEG-b-PBLG 4	13	9.69	1.12	88 (0.17)

[a] Solids content. [b] Absolute number average molar mass (Mn) and dispersity (Đ) determined by SEC using a multi-angle static light scattering detection. [c] Hydrodynamic diameter (Dh) and dispersity (σ) determined using a Malvern apparatus

Keeping the same initiator to monomer ratio, while decreasing the solids content τ_s to 4% gave copolymers with similar molar mass and dispersity as evidenced by the GPC curves (Fig 3). Increasing the solids content, up to 130 mg/mL (τ_s = 13 %), resulted in diblock copolymers with also similar molar masses (τ_s = 10%: M_n = 9.94 kDa and $Đ$ = 1.09; τ_s = 13 %: M_n = 9.69 kDa and $Đ$ = 1.12, Fig 3). Attempts to perform aqueous ROPISA at even higher solid content affords soft gels and incomplete conversions (data not showed). At all solids contents below or equal to τ_S = 13%, particles size and distributions are essentially unchanged as compared to τ_s = 7% (Fig 3, Table 1). Overall, the ROPISA of BLG-NCA initiated by PEG_{5K} is a facile and robust process to prepare well-defined amphiphilic polypeptide in aqueous solution and to access their related nanomaterials at unprecedented solids content with high reproducibility. Importantly, the known two-step kinetic process of the NCA-ROP[22] and the strong influence of the secondary structure on the self-assembly process[24] are two critical features that could significantly impact the behavior of the proposed aqueous ROPISA of NCA.

C. Grazon, P. Salas-Ambrosio, E. Ibarboure, A. Buol, E. Garanger, M.W. Grinstaff, S. Lecommandoux, C. Bonduelle, Angewandte Chemie International Edition 2019. DOI 10.1002/anie.201912028

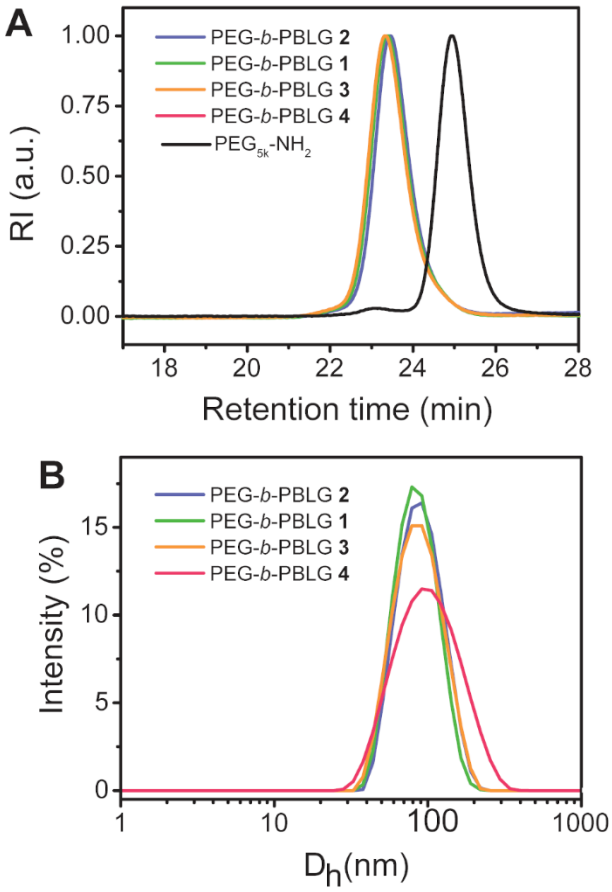

Figure 3. Solid content (τ_s) effect on the PEG-*b*-PBLG synthesis by ROPISA ([M]/[I] = 19) PEG-*b*-PBLG **2**, τ_s = 4%, PEG-*b*-PBLG **1**, τ_s = 7%, PEG-*b*-PBLG **3**, τ_s = 10%, PEG-*b*-PBLG **4**, τ_s = 13%: A. Steric exclusion chromatogram in DMF (1mg/mL LiBr, RI detection). B. Hydrodynamic diameter distribution measured by DLS in MQ water.

Next, we studied the nanoparticles obtained by the ROPISA process by atomic force microscopy (AFM) and Cryo-TEM (Fig 4). Cryo-TEM analysis was undertaken to observe the morphology of the nanoparticles in their hydrated state. Nanoparticles obtained at [M]/[I] = 19 and at τ_s = 7% are homogeneous in size and morphologies with needle-like structures (Figure 4 A and B). FTIR analysis of the lyophilized nanoparticles powder shows that a significant amount of the polypeptide adopts β-sheet and α-helix conformation (Fig SI 17) and we therefore propose that this original nanoparticle morphology is linked to the secondary structure of the polypeptide block. AFM images of the same particles, recorded in the dried state, (Fig 4B and SI 16) confirm the presence of separated and individual nanorods nanoparticles with homogeneous lengths (65 ± 10 nm) and diameters (4.2 ± 0.5 nm). Light scattering measurements (Fig SI 15) also confirm the elongated shape of the particles with a R_G/R_H = 1.5. Cryo-TEM images of the materials obtained from the second feed experiment (PEG-*b*-PBLG **6**, Fig 4 D) reveal that when the PBLG molar mass increases ([M]/[I] = 35), the nanorod morphology evolves to worm-like morphology, this known and characteristic morphology explaining the soft gel state observed in some of our ROPISA experiments. Note here that a control experiment of ROPISA in pure water (PEG-*b*-

PBLG **5**, [M]/[I] = 19 and at τ_s = 7%) also results in worm-like morphologies but the corresponding diblock copolymers are more disperse (Fig 4E and SI 2).

Finally, ROPISA of BLG-NCA was performed with a larger amino-PEG initiator (PEG-*b*-PBLG 7, [M]/[I] = 38 using PEG_{10k}-NH_2, Fig SI 5, 9 and 18). Upon ROP, well-defined amphiphilic polypeptides are also obtained as observed by ^{1}H NMR and SEC analyses. Cryo-TEM images also show worm-like morphologies. To further expand the versatility of the system, we also synthesized a diblock copolymer PEG-*b*-P(*NBoc*Lys) (Fig SI 6, 10 and 19). The obtained copolymer exhibits a similar molar mass and a narrow dispersity (M_n = 11.8 kDa, $Đ$ = 1.09, PS calibration). The ROPISA process is amenable to be used with different macroinitiators and NCA monomers. The minimal amount of spherical morphologies obtained in all these different examples support the hypothesis that ROPISA of NCA monomers is strongly influenced by the secondary structure of the polypeptides, a unique feature of this PISA process.

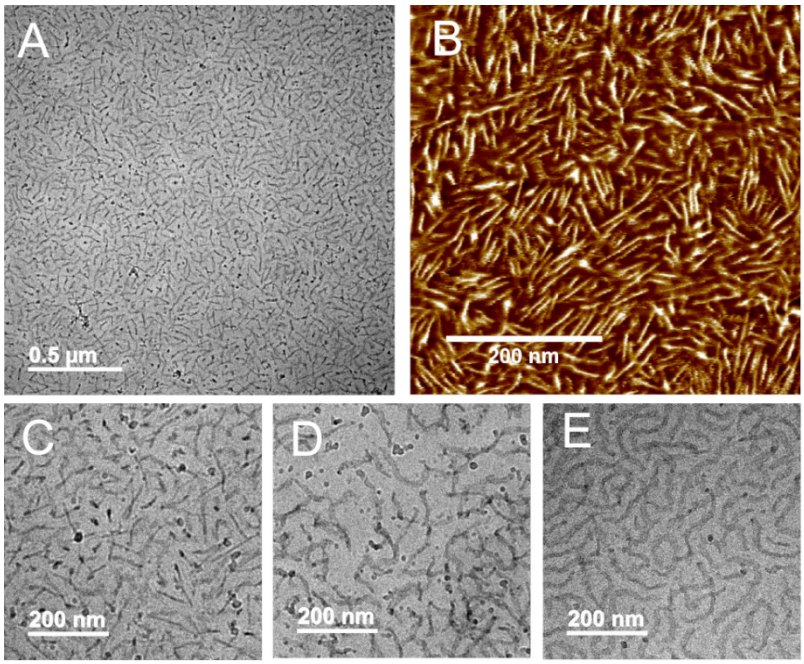

Figure 4. Needles and worm-like morphologies obtained upon aqueous ROPISA. A (scale bar = 0.5 µm), C, D, E (scale bar = 0.2 µm): Cryo-TEM image and B: AFM imaging upon drying (scale bar = 0.2 µm). A, B, C: PEG-*b*-PBLG **1** using PEG_{5k}-NH_2 as an initiator and [M]/[I] = 19. D. PEG-*b*-PBLG **6** using PEG_{5k}-NH_2 as an initiator and [M]/[I] = 38. E. PEG-*b*-PBLG **5** using PEG_{5k}-NH_2 as an initiator in MQ water.

In summary, we present an efficient process to obtain highly concentrated polymeric nanomaterials from ROP of NCA monomers in aqueous solution. The method is facile, highly reproducible, and time-saving, as well as allows high solids content in comparison to previous formulation methods like co-precipitation or emulsions processes. The proposed ROPISA utilizes the unprecedented reactivity of NCA monomers in aqueous solution, where they are rarely used because of rapid hydrolysis. This first-in-kind study demonstrates that ring-opening polymerization of hydrophobic *N*-carboxyanhydride monomers using hydrophilic macroinitiators

produces well-defined amphiphilic copolypeptides and nano- structures. It establishes the use of a single step reaction to overcome the challenges with aqueous ROP of NCA monomers. Further, through judicious choice of both the initiator and the NCA monomer specific nano-structures are prepared, highlighting how chemical design influences the self-assembly process and resulting nanomaterials.

Experimental Section

Experimental Details are available and contains material and methods, as well as polymers and nanoparticle characterizations (NMR, SEC, FTIR, DLS, SLS, microscopy images).

Acknowledgements

The authors acknowledge Amelie Vax and Sylvain Bourasseau for assistance with size-exclusion chromatography and Jean Michel Guigner for assistance with CRYO-TEM analyses. CG received support from a Marie-Curie fellowship from the European Union under the program H2020, Grant 749973. PSA received support from CONACYT (scholarship holder No. 548662)

Keywords: amphiphiles• polymerization • self-assembly • synthetic methods • water

---

[1] a) C. Wang, Z. Wang, X. Zhang *Acc. Chem. Res.* **2012**, *45*, 608-618. b) T. Terashima, In *Reversible Deactivation Radical Polymerization: Materials and Applications*, Vol. 1285, American Chemical Society: **2018**, p 143-155.

[2] E. Garanger, S. Lecommandoux *Angew. Chem. Int. Ed.* **2012**, *51*, 3060-3062.

[3] I.W. Hamley *Soft Matter* **2011**, *7*, 4122-4138.

[4] a) L. Sun, C. Zheng, T.J. Webster *Int. J. Nanomed.* **2017**, *12*, 73-86. b) C. Cai, J. Lin, Y. Lu, Q. Zhang, L. Wang *Chem. Soc. Rev.* **2016**, *45*, 5985.

[5] a) N. Hadjichristidis, H. Iatrou, M. Pitsikalis, G. Sakellariou *Chem. Rev.* **2009**, *109*, 5528-5578. b) T.J. Deming *Macromolecules* **1999**, *32*, 4500-4502.

[6] J.R. Kramer, T.J. Deming *Biomacromolecules* **2010**, *11*, 3668-3672.

[7] H.R. Kricheldorf *Angew. Chem. Int. Ed.* **2006**, *45*, 5752-5784.

[8] T.J. Deming In *Peptide Hybrid Polymers*, (Klok, H.-A., Schlaad, H., Eds.), Springer Berlin Heidelberg: Berlin, Heidelberg, **2006**, p 1-18.

[9] Z. Song, Z. Han, S. Lu, C. Chen, L. Chen, L. Yin, J. Cheng *Chem. Soc. Rev.* **2017**, 46, 6570-6599.

[10] J. Zou, J. Fan, X. He, S. Zhang, H. Wang, K. Wooley *Macromolecules* **2013**, *46*, 4223-4226.

[11] a) W. Zhao, Y. Gnanou, N. Hadjichristidis *Chem. Commun.* **2015**, *51*, 3663-3666. b) W. Zhao, Y. Gnanou, N. Hadjichristidis *Biomacromolecules*, **2015**, *16*, 1352-1357.

[12] Y. Wu, D. Zhang, P. Ma, R. Zhou, L. Hua, R. Liu *Nature Comm.* **2018**, *9*, 5297.

[13] Z. Song, H. Fu, J. Wang, J. Hui, T. Xue, L.A. Pacheco, H. Yan, R. Baumgartner, Z. Wang, Y. Xia, X Wang, L. Yin, C. Chen, J. Rodríguez-López, A. Ferguson, Y. Lin, J. Cheng *Proc. Nat. Acad. Sci.* **2019**, *116*, 10658-10663.

[14] J. Huang, C. Bonduelle, J. Thévenot, S. Lecommandoux, A. Heise *J. Am. Chem. Soc.* **2012**, *134*, 119-122.

[15] R. Tong, J. Cheng *J. Am. Chem. Soc.* **2009**, *131*, 4744-4754.

[16] J. Jacobs, D. Pavlovic, H. Prydderch, M.A. Moradi, E. Ibarboure, J.P.A. Heuts, S. Lecommandoux, A. Heise *J. Am. Chem. Soc.* **2019**, 141, 12522-12526.

[17] a) N.J. Warren, S.P. Armes *J. Am. Chem. Soc.* **2014**, *136*, 10174-10185. b) F. D'Agosto, J. Rieger, M. Lansalot Angew. Chem. Int. Ed. **2019**, doi 10.1002/anie.201911758.

[18] J. Yeow, O.R. Sugita, C. Boyer *ACS Macro Letters* **2016**, *5*, 558-564.

[19] a) M.R. Hill, E. Guégain, J. Tran, C.A. Figg, A.C Turner, J. Nicolas, B.S. Sumerlin *ACS Macro Lett.* **2017**, *6*, 1071-1077. b) J. Jiang, X. Zhang, Z. Fan, J. Du *ACS Macro Lett.* **2019**, 8, 1216-1221.

[20] a) P.D. Barlett, D.C Dittmer *J. Am. Chem. Soc.* **1957**, *79*, 2159-2160. b) P.D. Barlett, R.H. Jones *J. Am. Chem. Soc.* **1957**, *79*, 2153-2159.

[21] a) R. Hirschmann, R.G. Strachan, H. Schwam, E.F. Schoenewaldt, B. Joshua, B. Barkemeyer, D.F. Veber, W.J. Paleveda, T.A. Jacob, T.E. Beesley, R.G. Denkewalter *J. Org. Chem.* **1967**, *32*, 3415-3425. b) R. Plasson, J.P. Biron, H. Cottet, A. Commeyras, J. Taillades *J. Chromatogr. A* **2002**, *952*, 239-248. c) H. Collet, E. Souaid, H. Cottet, A. Deratani, L. Boiteau, G. Dessalces, J.C. Rossi, A. Commeyras, R. Pascal *Chem. Eur. J.* **2010**, *16*, 2309-2316.

[22] C. Chen, H. Fu, R. Baumgartner, Z. Song, Y. Lin, J. Cheng *J. Am. Chem. Soc.* **2019**, *141*, 8680-8683.

[23] a) A. Blanazs, J. Madsen, G. Battaglia, A.J. Ryan, S.P. Armes *J. Am. Chem. Soc.* **2011**, *133*, 16581-16587. b) I. Chaduc, M. Girod, R. Antoine, B. Charleux, F. D'Agosto, M. Lansalot, *Macromolecules* **2012**, 45, 5881-5893.

[24] C. Bonduelle, *Polym. Chem.* **2018**, 9, 1517-1529.

SUPPORTING INFORMATION

Experimental Procedures

Materials

All chemicals were purchased from Sigma-Aldrich and used as received unless otherwise noted. γ-Benzyl-L-glutamate *N*-carboxyanhydride (BLG-NCA) and ε-tert-butyloxycarbonyl-L-lysine *N*-carboxyanhydride (*NBoc*Lys-NCA) were supplied from Isochem. PEG_{5k}-NH_2 (M_p = 5516, $Đ$ = 1.02), PEG_{10k}-NH_2 (M_p = 11153 Da, $Đ$ = 1.05) were bought from RAPP Polymer.

Methods

^{1}H spectra were recorded at room temperature with a Bruker Avance 400 (400 MHz). DMF-d_7 or $CDCl_3$ with 15% TFA were used as solvents and signals were referred to the signal of residual protonated solvent signals. TMS was used as an internal standard. Molar masses were determined using the following equation:

$$M_{n,\ PEG-b-PBLG} = \frac{H_{BLG}}{H_I} M_{BLG} + M_I \qquad \text{(eq. 1)}$$

Where H_{BLG} is the proton-normalized average intensity of the BLG signals (a: 2H, b: 2H, c: 2H and d: 1H, Figure SI-7), H_I is the proton-normalized intensity of the mPEG-NH_2 (f, g: 4H, Figure SI-7), M_{BLG} and M_I are, respectively, the molar mass of the BLG monomer unit and the molar mass of mPEG-NH_2 initiator. The obtained [M]/[I]=H_{BLG}/H_I and M_n values are summarized in Table SI-1 and given with a 10% error. The molar masses can also be estimated with eq 1 but using the terminus CH_3 (h: 3H, Figure SI-7) of the mPEG-NH2 instead. Those second [M]/[I] are also summarized in Table SI-1 in brackets.

Fourier Transformed Infrared Spectroscopy – Attenuated (FTIR-ATR). FTIR spectra were collected on a Bruker Vertex 70 in the spectral region of 900-2000 cm^{-1} and were obtained from 32 scans with a resolution of 4 cm^{-1}. A background was recorded before loading the samples onto the ATR unit for measurements. FTIR of copolymers dialyzed and lyophilized powders were measured using air as a background. For the kinetic measurements, the dispersion was directly deposed on the ATR crystal after recording a background of $NaHCO_3$ in ultra-pure water.

Steric Exclusion Chromatography (SEC). Polymer molar masses were determined by SEC using dimethyformamide (DMF + LiBr 1g/L) as the eluent. Measurements in DMF were performed on an Ultimate 3000 system from Thermoscientific equipped with diode array detector DAD. The system also include a multi-angles light scattering detector MALS and differential refractive index detector dRI from Wyatt technology. Polymers were separated on three Shodex Asahipack gel columns [GF-1G 7B (7.5 × 8 mm), GF 310 (7.5 × 300 mm), GF510 (7.5×300), exclusion limits from 500-300 000 Da] at a flowrate of 0.5 mL/min. Columns temperature was held at 50°C. Easivial kit of Polystyrene from Agilent was used as the standard (Mn from 162 to 364 000 Da).

C. Grazon, P. Salas-Ambrosio, E. Ibarboure, A. Buol, E. Garanger, M.W. Grinstaff, S. Lecommandoux, C. Bonduelle, Angewandte Chemie International Edition 2019. DOI 10.1002/anie.201912028

Individual offline batch-mode measurements were performed to determine the homopolymers accurate Refractive index increment (*dn/dc*) values in DMF + LiBr 1g/L at 50°C. Various polymer concentrations were prepared and injected at 0.6mL per minutes in dRI from Wyatt Technology. Differential refractive index data were obtained for each solution and plotted versus concentration using the Wyatt Astra VI software.

Homopolymer	*dn/dc* (mL/g)
PEG5k-NH2	0.0460
PBLG	0.1125

For the block copolymers, the *dn/dc* values were estimated using the following equation (Polymer Handbook, 4th Edition, Wiley 1999):

$$\frac{dn}{dc} = w_A(\frac{dn}{dc})_A + w_B(\frac{dn}{dc})_B \quad \text{(eq. 2)}$$

Where w_A and w_B are the weight fractions of monomers A and B and *dn/dc* their respective refractive index increment.

Atomic Force Microscopy (AFM) measurements were performed at room temperature in a dry state using a Multimode 8™ microscope (Veeco Instruments Inc.). Both topographic and phase images of needle-like nanoparticles were obtained in Tapping Mode ™ using rectangular silicon cantilever (AC 160-TS, Atomic Force, Germany) with a spring constant of 26N m^{-1}, a resonance frequency lying in the 270-320 kHz range and a radius of curvature of less than 10 nm. Samples were prepared by solvent casting at ambient temperature from a stock solution (70 mg/ml). A drop (5µl) of suspension was deposited onto freshly cleaved mica and after 10 minutes the excess of solution was removed with blotting paper. Subsequently, the substrate was dried under nitrogen flow during several minutes. Measurements of length and width were taken using the section Particle Analysis tool provided with the AFM software (Nanoscope Analysis V1.20 from Bruker).

CryoTEM Cryo-Transmission Electron Microscopy (cryo-TEM) micrographs were obtained as follows: a drop of suspension was deposited on a "Quantifoil"® (Quantifoil Micro Tools GmbH, Germany) carbon membrane. The excess of liquid on the membrane was absorbed with filter paper and the membrane was quench-frozen quickly in liquid ethane to form a thin vitreous ice film including NPs in the holes of the grid. Once placed in a Gatan 626 cryo-holder cooled with liquid nitrogen, the samples were transferred into the microscope and observed at low temperature (−180 °C). Cryo-TEM images were recorded on an Ultrascan 2k CCD camera (Gatan, USA), using a LaB6 JEOL 2100 (JEOL, Japan) cryo microscope operating at 200 kV with a JEOL low dose system (Minimum Dose System, MDS) to protect the thin ice film from any irradiation before imaging and reduce the irradiation during the image capture.

Dynamic Light Scattering (DLS) The hydrodynamic diameter (D_h) and the dispersity (σ) of the nanoparticles were determined by DLS with a Zetasizer Nano ZS from Malvern Instruments operating with a He–Ne laser source (wavelength 633 nm, scattering angle 90°). The correlation functions were analysed using the cumulant method. The dispersions were analysed at 0.1 wt % in MQ water after filtration on a 1µm glass filter.

Multi-angle Dynamic and Static Light Scattering (DLS - SLS) Multiangle dynamic and static light scattering experiments were performed using an ALV/CGS3 compact goniometer equipped with an ALV/LSE-5004 light scattering electronics and an ALV-7004 multi tau digital correlator with pseudo-cross correlation detection. The light source was a 22mW He-Ne laser operating at λ=632.8 nm. The accessible scattering angles ranged from 50° to 130°. The nanoparticles dispersions were prepared at 0.1 wt % in ultra-pure water and filtered through 1 µm glass filter before analysis. Samples (1 mL in 1 cm-diameter cylindrical glass cells) were immersed in a filtered toluene bath and equilibrated for 2 min at 25 °C. Static and dynamic data of 6 independent 10 s-measurements were recorded with the ALV-correlator control software. The autocorrelation functions (*g(t)*) were analyzed in terms of relaxation time distribution (*τ*) (equation 3):

$$g(t) = \int A_{(\tau)} exp\,(\frac{-t}{\tau}) d\tau \qquad \text{(eq. 3)}$$

The hydrodynamic radius (R_h) was calculated from the diffusion coefficient (D) using the Stokes−Einstein relation:

$$D = \frac{k_B T}{6\pi\eta_S R_H} \qquad \text{(eq. 4)}$$

where D is calculated from the slope of the curve $1/\tau$ as a function of q^2. τ is the main correlation time determined by the second order cumulant analysis of the autocorrelogram, q the scattering vector defined as $q = (4\pi/\lambda)\sin(\theta/2)$ with λ the wavelength and θ the scattering angle, k_B the Boltzmann constant, T the temperature in Kelvin and η_S the viscosity of the solvent.

Radii of gyration (R_G) were determined from the plot of $\ln I(q)$ as a function of q^2 using the Guinier approximation:

$$\ln I(q) = \ln I\,(0) - \frac{q^2 R_G^2}{3} \qquad \text{(eq. 5)}$$

Where $R_G^2/3$ corresponds to the slope of the curve.

C. Grazon, P. Salas-Ambrosio, E. Ibarboure, A. Buol, E. Garanger, M.W. Grinstaff, S. Lecommandoux, C. Bonduelle, Angewandte Chemie International Edition 2019. DOI 10.1002/anie.201912028

Synthesis procedures

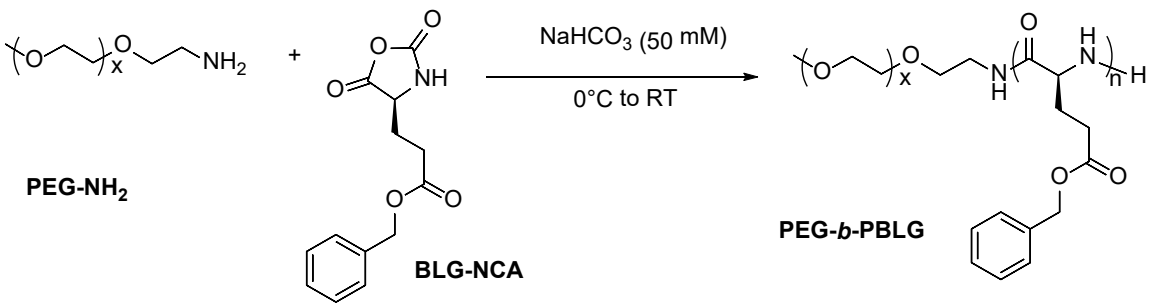

Scheme SI 1: Poly(ethylene glycol)-*b*-poly(γ-benzyl-L-glutamate) synthesis

Typical synthesis procedure of poly(ethylene glycol)-*b*-poly(γ-benzyl-L-glutamate)

In a glove box, the NCA monomer of γ-benzyl-L-glutamate (300 mg, 1.14 mmol) is weight in a Schlenk tube containing a magnetic stirring bar. The Schlenk is removed from the glove box and cooled on ice. 8mL of an ice-cooled solution of $NaHCO_3$ 0.05M containing the initiator PEG_{5k}-NH_2 (300mg, 0.06 mmol, [M]/[I] = 19) is added to the BLG-NCA powder under a strong agitation (τ_s = 7%). The reaction is left to stir 1) first in an ice-cold water bath; 2) then at room temperature overnight. The opalescent dispersion obtained is then transferred to a 3.5 kDa dialysis membrane and dialysed against deionised water for 2 days. An aliquot is kept for further microscopy imaging and dynamic light scattering and the remaining dispersion is lyophilized. A white powder is obtained with a yield of 85 ± 3%.

PEG_{10k}-NH_2 was also used as an initiator using the same protocol. In this case, 600 mg of initiator and 600 mg of BLG-NCA were used, as such increasing [M]/[I] = 38. The solids content was τ_s = 13%.

Solids content effect (τ_s)

The protocol as described above was slightly modified to change the solid content of the reaction. To proceed, the ratio [M]/[I] was kept constant ([M]/[I] = 19) but the amount of $NaHCO_3$ 0.05M buffer solution was adjusted to reach a τ_s = 4%, 7% (typical procedure), 10% or 13%.

Chain extension

In a glove box, the NCA monomer of γ-benzyl-L-glutamate (300 mg, 1.14 mmol) is weight in a Schlenk tube containing a magnetic stirring bar. The Schlenk is removed from the glove box and cooled on ice. 8mL of an ice-cooled solution of $NaHCO_3$ 0.05M containing the initiator PEG_{5k}-NH_2 (300mg, 0.06 mmol, [M]/[I] = 19) is added to the BLG-NCA powder under a strong agitation (τ_s = 7%). After 90 min, a second feed of BLG-NCA (300mg, 0.06 mmol, [M]/[I] = 38, τ_s = 13%) is performed by adding directly the monomer powder to the dispersion. The reaction is left to stir at room temperature overnight. The dispersion obtained is then transferred to a 3.5 kDa dialysis

C. Grazon, P. Salas-Ambrosio, E. Ibarboure, A. Buol, E. Garanger, M.W. Grinstaff, S. Lecommandoux, C. Bonduelle, Angewandte Chemie International Edition 2019. DOI 10.1002/anie.201912028

membrane and dialysed against deionised water for 2 days. An aliquot is kept for further microscopy imaging and dynamic light scattering and the remaining dispersion is lyophilized. A white powder is obtained with a yield of 85 %.

Typical synthesis procedure of poly(ethylene glycol)-*b*-poly(ε-tert-butyloxycarbonyl-L-lysine)

In a glove box, the NCA monomer of ε-tert-butyloxycarbonyl-*L*-lysine *N*-carboxyanhydride (*NBoc*Lys-NCA, 310 mg, 1.14 mmol) is weight in a Schlenk tube containing a magnetic stirring bar. The Schlenk is removed from the glove box and cooled on ice. 8mL of an ice-cooled solution of $NaHCO_3$ 0.05M containing the initiator PEG_{5k}-NH_2 (300mg, 0.06 mmol, [M]/[I] = 19) is added to the *NBoc*Lys-NCA powder under a strong agitation (τ_s = 7%). The reaction is left to stir 1) first in an ice-cold water bath; 2) then at room temperature overnight. The opalescent dispersion obtained is then transferred to a 3.5 kDa dialysis membrane and dialysed against deionised water for 2 days. An aliquot is kept for further microscopy imaging and dynamic light scattering and the remaining dispersion is lyophilized. A white powder is obtained.

Kinetic study

The chain extension of PEG-*b*-PBLG was followed by a kinetic study. The same protocol as described above is used for the ROPISA. In a glove box, the NCA monomer of γ-benzyl-L-glutamate (300 mg, 1.14 mmol) is weight in a Schlenk tube containing a magnetic stirring bar. The Schlenk is removed from the glove box and cooled on ice. 8mL of an ice-cooled solution of $NaHCO_3$ 50mM containing the initiator PEG_{5k}-NH_2 (300mg, 0.06 mmol, [M]/[I] = 19) is added to the BLG-NCA powder under a strong agitation. The reaction is left to stir in an ice-cold water bath overnight. At different time points, an aliquot of 500 µL of dispersion is quenched by adding 8 mg of fluorescein isothiocyanate (FITC) in 500 µL of DMSO. The mixture is vortexed and dialysed against water on 3.5 kDa membrane for 3 days. The aliquots are then lyophilized and analysed by ^{1}H NMR in $CDCl_3$ and by SEC in DMF (+ 1mg/mL of LiBr).

The formation of nanoobjects was also tracked by FTIR. In a typical reaction, 60 mg of γ-benzyl-*L*-glutamate is weight in a 5 mL vial containing a magnetic stirring bar in the glove box. Once removed from the glove box, the vial is chilled on ice and 1.6 mL of an ice-cold solution at 50 mM of $NaHCO_3$ in H_2O containing 30 mg of PEG_{5k}-NH_2 ([M]/[I] = 19) is added. At different time points, 5 µL of the dispersion is deposed directly on the ATR crystal.

Results and Discussion

Steric Exclusion chromatograms

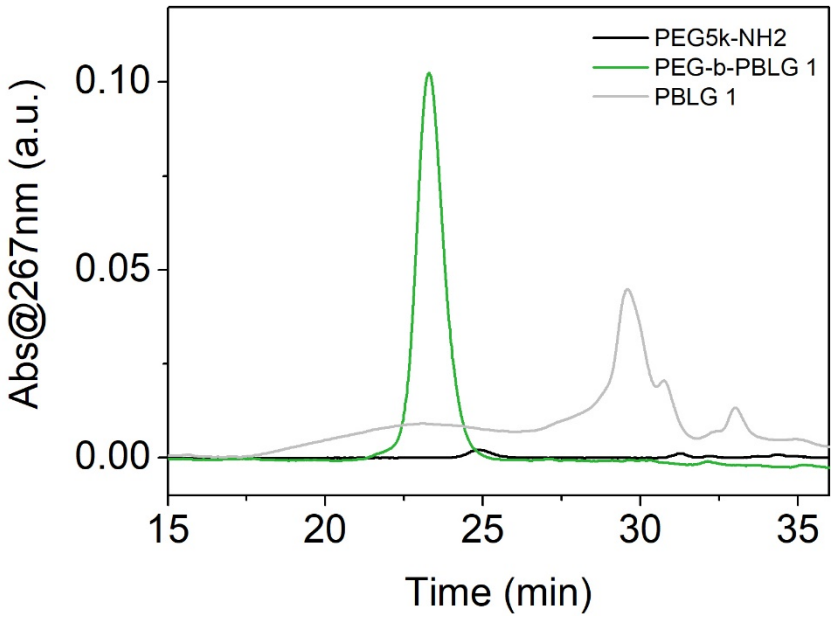

Figure SI 1 Steric exclusion chromatograms in DMF (1mg/mL LiBr, detection by absorption) of PEG-*b*-PBLG **1** ([M]/[I] = 19, τ_s = 7%), control PBLG **1** (only BLG in MQ water) and the reference PEG_{5k}-NH_2.

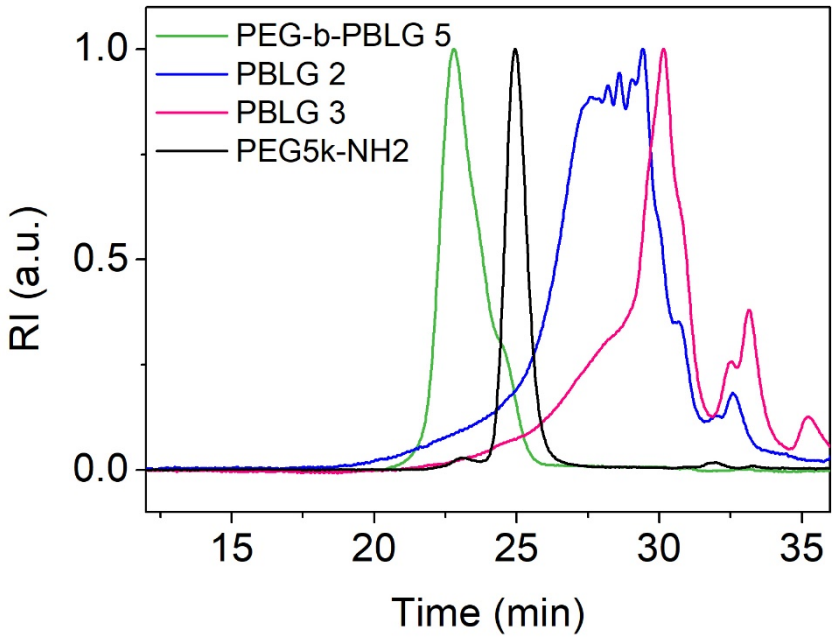

Figure SI 2 Steric exclusion chromatograms in DMF (1mg/mL LiBr) of PEG-*b*-PBLG **5** ([M]/[I] = 19, τ_s = 7%, MQ water) and controls PBLG **2** (I = Ethanolamine, [M]/[I] = 19, τ_s = 7%, $NaHCO_3$ 0.2M) and PBLG **3** (I = PEG_{5k}-OH, [M]/[I] = 19, τ_s = 7%, $NaHCO_3$ 0.2M).

C. Grazon, P. Salas-Ambrosio, E. Ibarboure, A. Buol, E. Garanger, M.W. Grinstaff, S. Lecommandoux, C. Bonduelle, Angewandte Chemie International Edition 2019. DOI 10.1002/anie.201912028

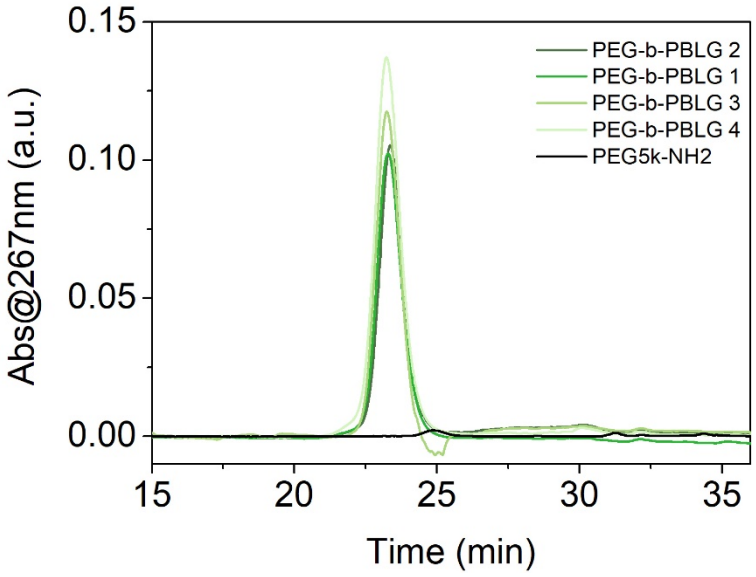

Figure SI 3 Solid content (τ_s) effect on the synthesis of PEG-*b*-PBLG by ROPISA ([M]/[I] = 19). PEG-*b*-PBLG **2**, τ_s = 4%, PEG-*b*-PBLG 1, τ_s = 7%, PEG-*b*-PBLG **3**, τ_s = 10%, PEG-*b*-PBLG **4**, τ_s = 13%. Steric exclusion chromatogram in DMF (1mg/mL LiBr, UV detection).

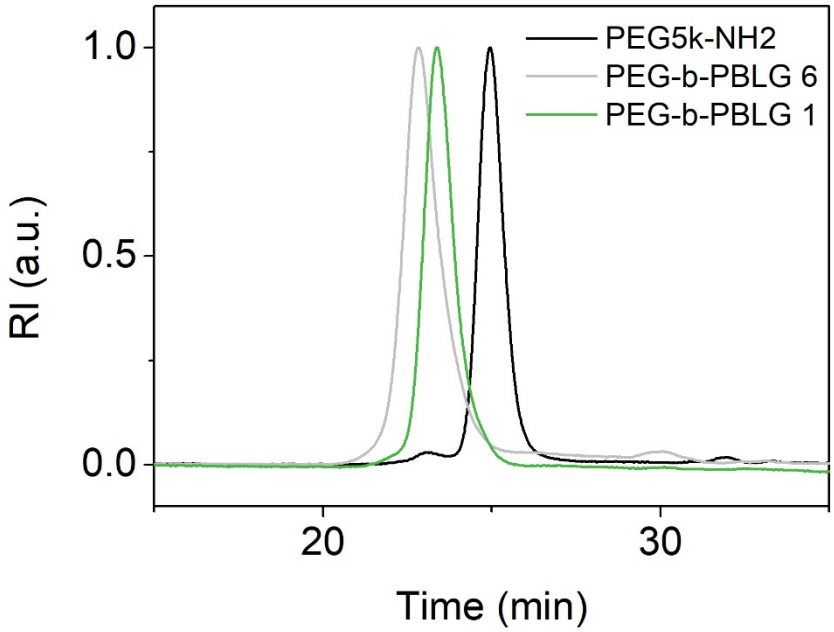

Figure SI 4 Steric exclusion chromatograms in DMF (1mg/mL LiBr) of PEG-*b*-PBLG **6** (2 feed of BLG-NCA).

C. Grazon, P. Salas-Ambrosio, E. Ibarboure, A. Buol, E. Garanger, M.W. Grinstaff, S. Lecommandoux, C. Bonduelle, Angewandte Chemie International Edition 2019. DOI 10.1002/anie.201912028

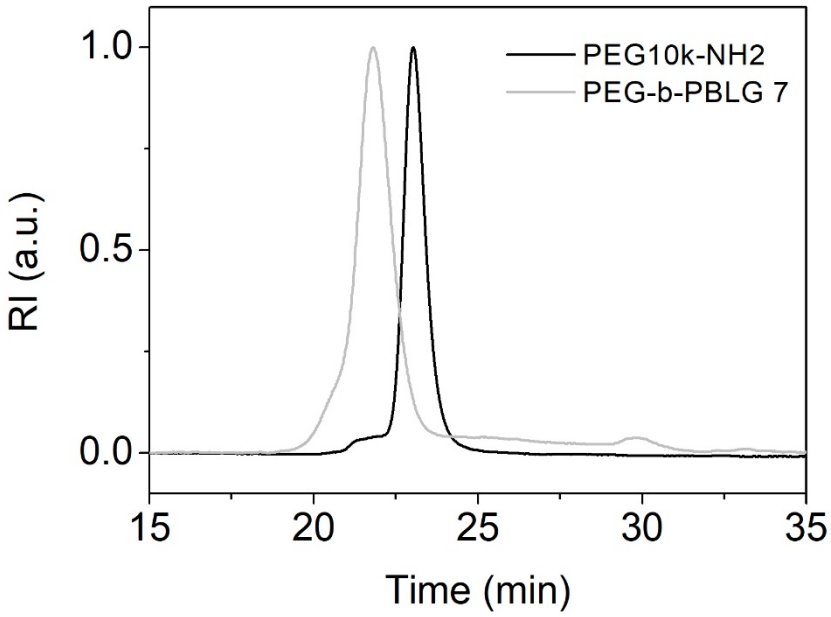

Figure SI 5 Steric exclusion chromatograms in DMF (1mg/mL LiBr) of PEG-*b*-PBLG **7** (I = PEG_{10k}-NH_2, [M]/[I] = 38, τ_s = 7%).

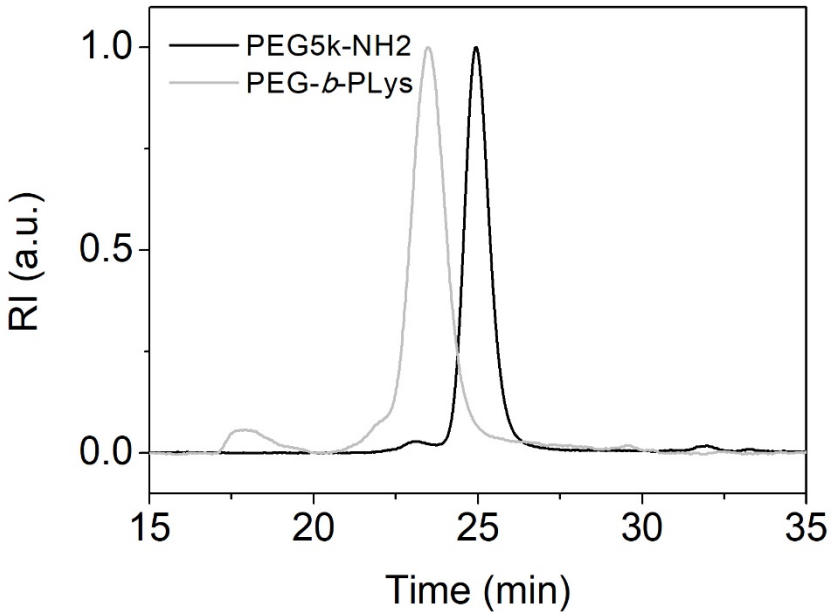

Figure SI 6 Steric exclusion chromatograms in DMF (1mg/mL LiBr) of PEG-*b*-P(*NBoc*Lys) (M = *NBoc*Lys-NCA, [M]/[I] = 19, τ_s = 7%).

C. Grazon, P. Salas-Ambrosio, E. Ibarboure, A. Buol, E. Garanger, M.W. Grinstaff, S. Lecommandoux, C. Bonduelle, Angewandte Chemie International Edition 2019. DOI 10.1002/anie.201912028

^{1}H NMR spectra

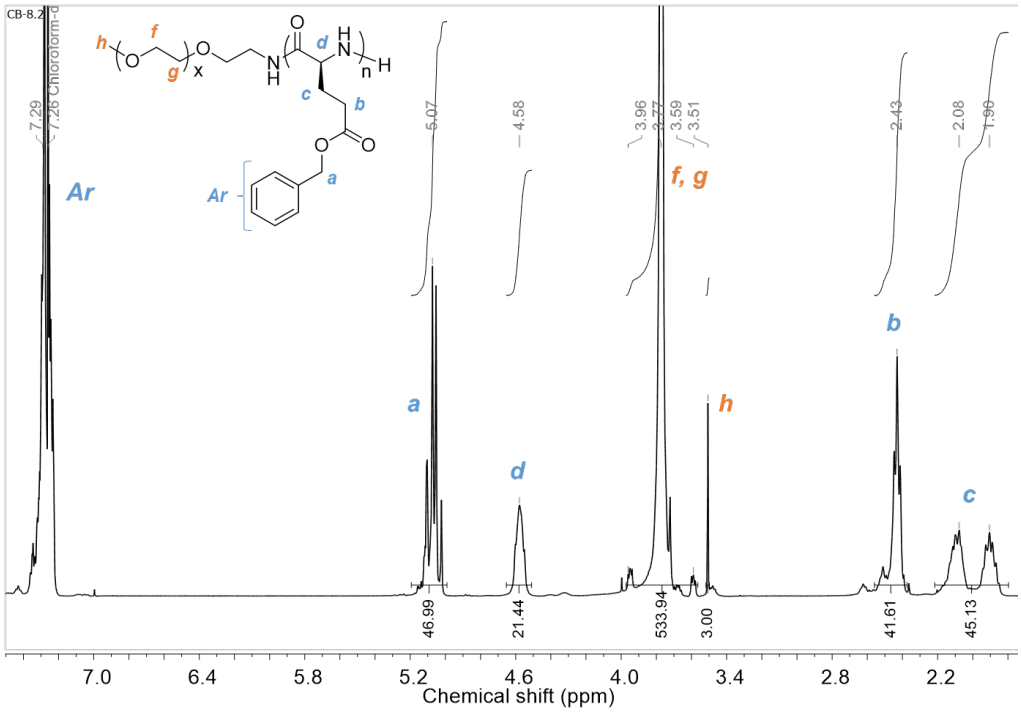

Figure SI 7 ^{1}H NMR spectra of PEG-*b*-PBLG **1** in $CDCl_3$ + 15% TFA.

C. Grazon, P. Salas-Ambrosio, E. Ibarboure, A. Buol, E. Garanger, M.W. Grinstaff, S. Lecommandoux, C. Bonduelle, Angewandte Chemie International Edition 2019. DOI 10.1002/anie.201912028

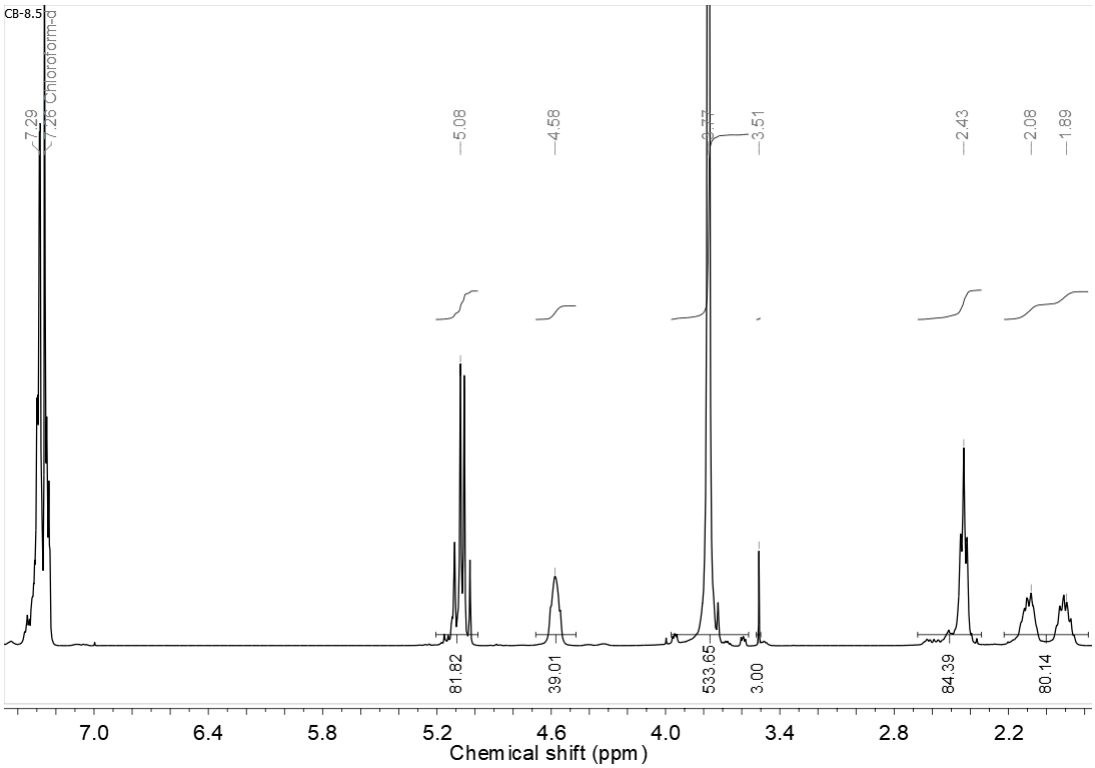

Figure SI 8 ^{1}H NMR spectra of PEG-*b*-PBLG **6** in $CDCl_3$ + 15% TFA.

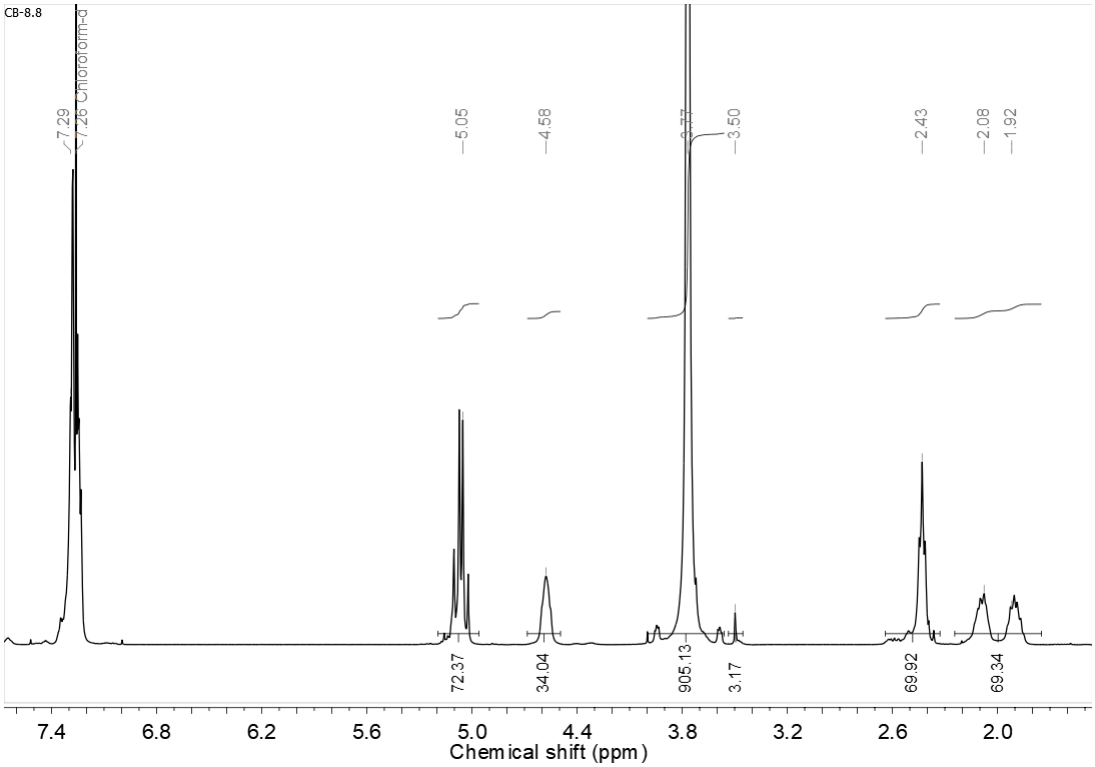

Figure SI 9 ^{1}H NMR spectra of PEG_{10k}-*b*-PBLG **7** in $CDCl_3$ + 15% TFA.

C. Grazon, P. Salas-Ambrosio, E. Ibarboure, A. Buol, E. Garanger, M.W. Grinstaff, S. Lecommandoux, C. Bonduelle, Angewandte Chemie International Edition 2019. DOI 10.1002/anie.201912028

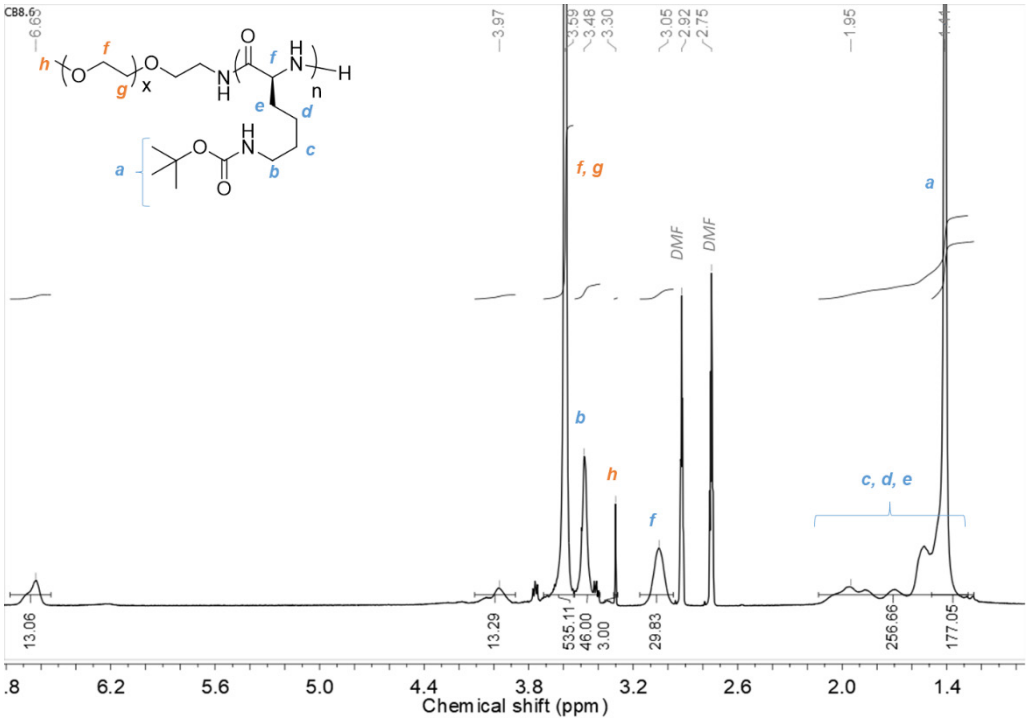

Figure SI 10 ^{1}H NMR spectra of PEG-*b*-P(*NBoc*Lys) in DMF-d7.

C. Grazon, P. Salas-Ambrosio, E. Ibarboure, A. Buol, E. Garanger, M.W. Grinstaff, S. Lecommandoux, C. Bonduelle, Angewandte Chemie International Edition 2019. DOI 10.1002/anie.201912028

Kinetic of the polymerization

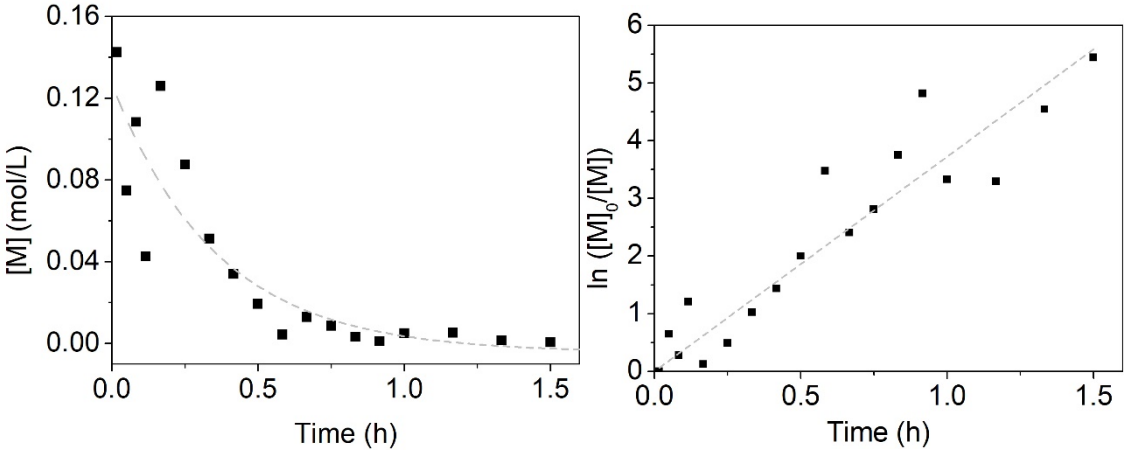

Figure SI 11 Kinetic study followed by FTIR (Abs@1880 cm^{-1}) of PEG_{5k}-NH_2 initiated BLG-NCA polymerization at a BLG-NCA:I molar ratio of 19:1 at 4°C. The initial BLG-NCA concentration was 0.14 M. Left: evolution of BLG-NCA concentration over time and fit using an exponential decay. Right: Logarithm of initial BLG-NCA concentration normalized by the BLG-NCA concentration over time. Slope of the linear equation: a = 0.00103 ± 5.6 x 10^{-5} s^{-1} = 3.72 ± 0.202 h^{-1}.

The polymerization rate (k) was obtained by plotting the natural logarithm of monomer concentration *versus* time and fitting of the data using equation 7:

$$\ln[M] = ln[M]_0 - k[I]_0 t \qquad \text{(eq. 6)}$$

$$k = -slope/[I]_0 \qquad \text{(eq. 7)}$$

The monomer conversion was determined by ATR-FTIR using the intensity of BLG-NCA anhydride absorption band at 1880 cm^{-1}.

C. Grazon, P. Salas-Ambrosio, E. Ibarboure, A. Buol, E. Garanger, M.W. Grinstaff, S. Lecommandoux, C. Bonduelle, Angewandte Chemie International Edition 2019. DOI 10.1002/anie.201912028

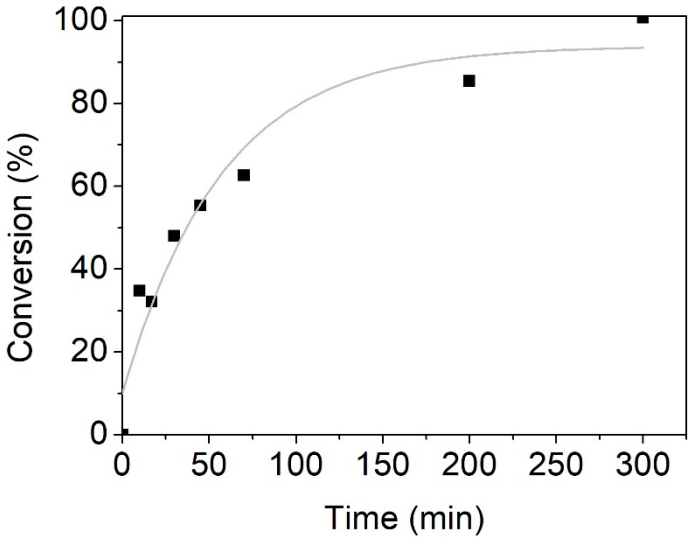

Figure SI 12 Kinetic study followed by ^{1}H NMR in $CDCl_3$ of PEG_{5k}-NH_2 initiated BLG-NCA polymerization at [M]/[I]=19, at 4°C. At each point of the kinetic, an aliquot of the reaction media is quenched using FITC.

C. Grazon, P. Salas-Ambrosio, E. Ibarboure, A. Buol, E. Garanger, M.W. Grinstaff, S. Lecommandoux, C. Bonduelle, Angewandte Chemie International Edition 2019. DOI 10.1002/anie.201912028

Light scattering

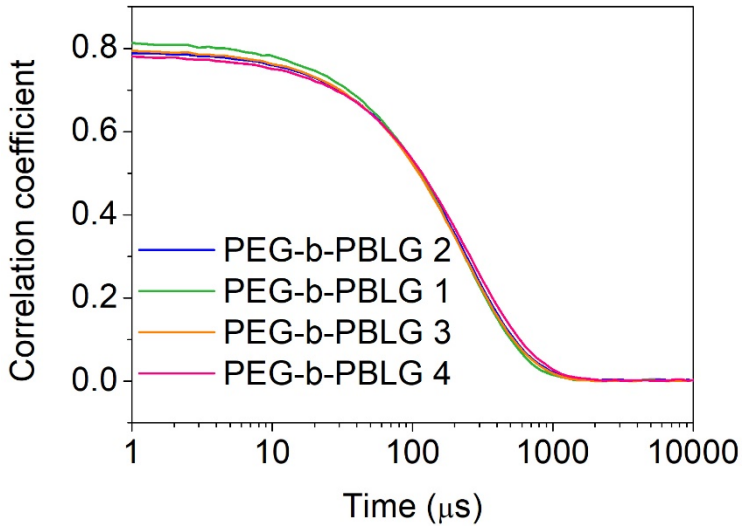

Figure SI 13 Solid content (τ_s) effect on the synthesis of PEG-*b*-PBLG by ROPISA ([M]/[I] = 19). PEG-*b*-PBLG **2**, τ_s = 4%, PEG-*b*-PBLG **1**, τ_s = 7%, PEG-*b*-PBLG **3**, τ_s = 10%, PEG-*b*-PBLG **4,** τ_s = 13%. Correlogram of the DLS.

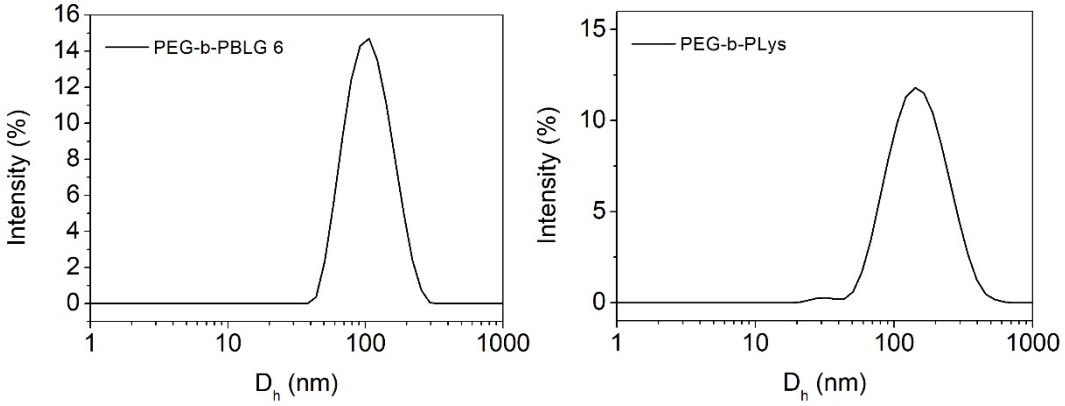

Figure SI 14 Versatility of the system. Distribution of hydrodynamic diameter observed by DLS. Left. PEG-*b*-PBLG **6** using PEG_{5k}-NH_2 as an initiator and [M]/[I] = 38. Right: PEG-*b*-P(*NBoc*Lys) using PEG_{5k}-NH_2 as an initiator and [M]/[I] = 19.

C. Grazon, P. Salas-Ambrosio, E. Ibarboure, A. Buol, E. Garanger, M.W. Grinstaff, S. Lecommandoux, C. Bonduelle, Angewandte Chemie International Edition 2019. DOI 10.1002/anie.201912028

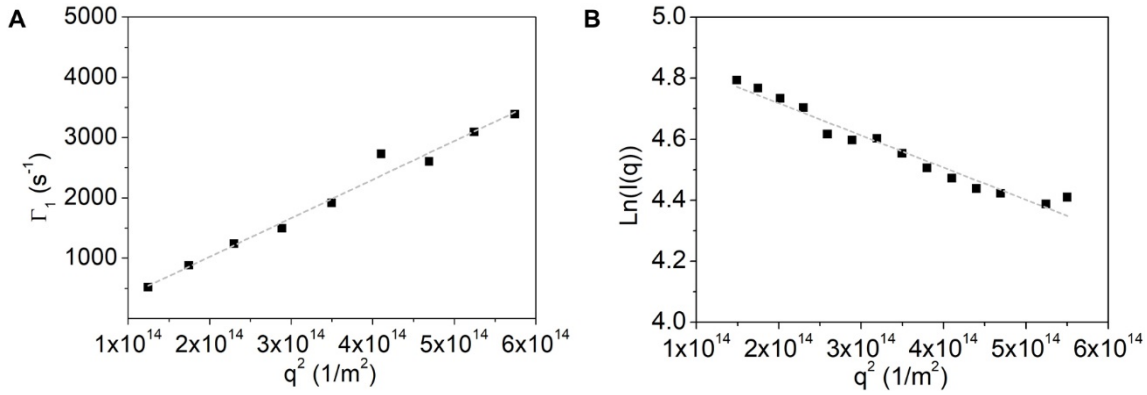

Figure SI 15 Static and Dynamic Light scattering plots of the sample PEG-*b*-PBLG **1** in ultra-pure water at 25°C. A: determination of the Hydrodynamic radius (slope of the fitted linear curve = 6.41 x 10^{-12} $m^2.s^{-1}$) and B: Guinier plot to determine the Giration radius (slope of the fitted linear curve = -8.00 x 10^{-16} m^2). We find R_H = 38.3 nm and R_G = 56.3 nm, *ie* R_G/R_H = 1.47.

Nanoparticles' structure characterization

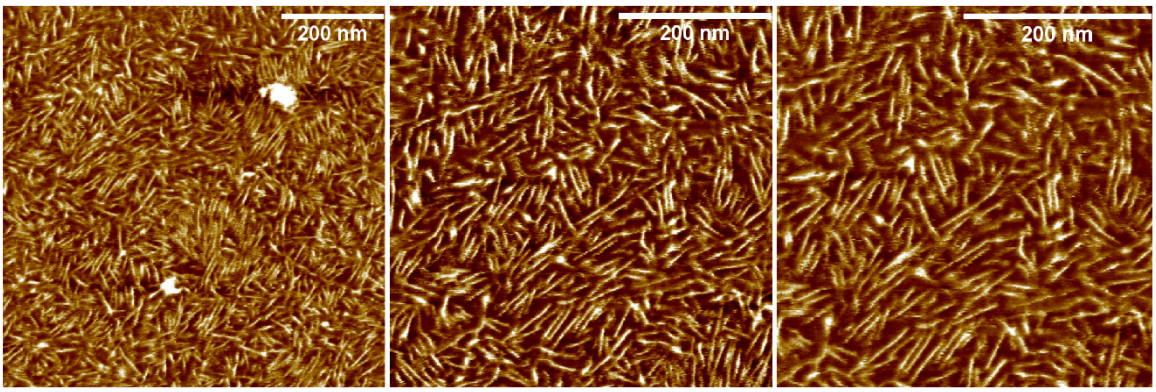

Figure SI 16 AFM images showing needle-like nanoparticles of the sample PEG-*b*-PBLG **1**.

C. Grazon, P. Salas-Ambrosio, E. Ibarboure, A. Buol, E. Garanger, M.W. Grinstaff, S. Lecommandoux, C. Bonduelle, Angewandte Chemie International Edition 2019. DOI 10.1002/anie.201912028

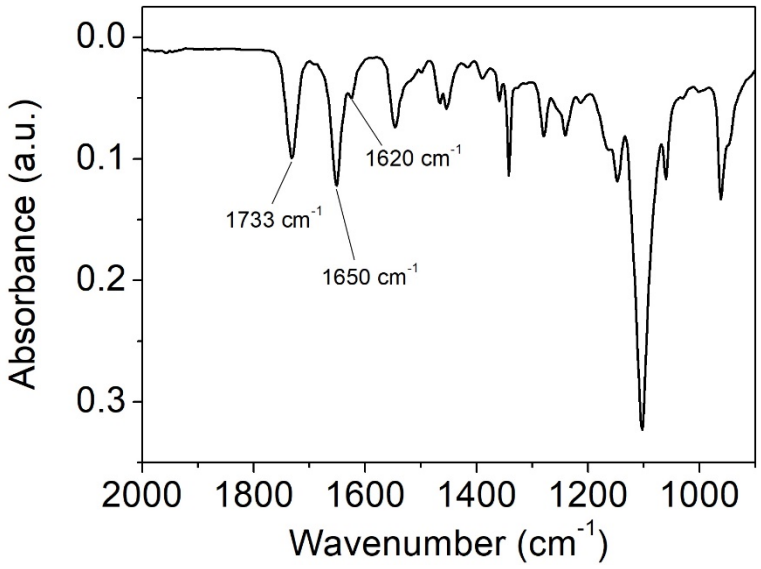

Figure SI 17 FTIR of the sample PEG-*b*-PBLG **1** lyophilized.

C. Grazon, P. Salas-Ambrosio, E. Ibarboure, A. Buol, E. Garanger, M.W. Grinstaff, S. Lecommandoux, C. Bonduelle, Angewandte Chemie International Edition 2019. DOI 10.1002/anie.201912028

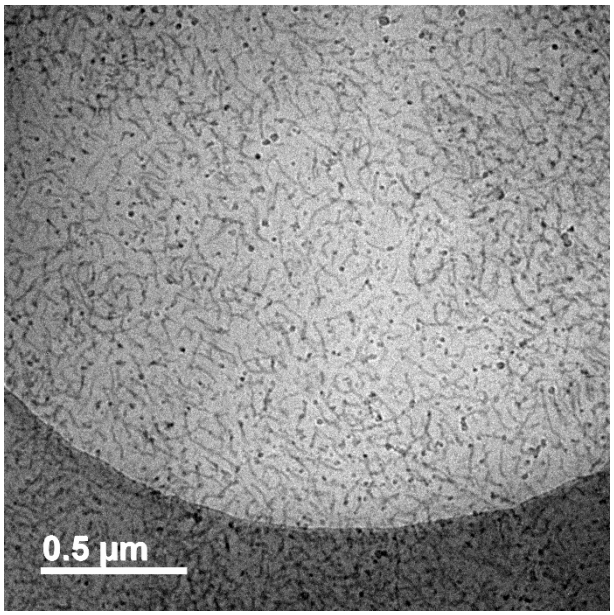

Figure SI 18 Cryo-TEM image of the sample PEG-*b*-PBLG 7.

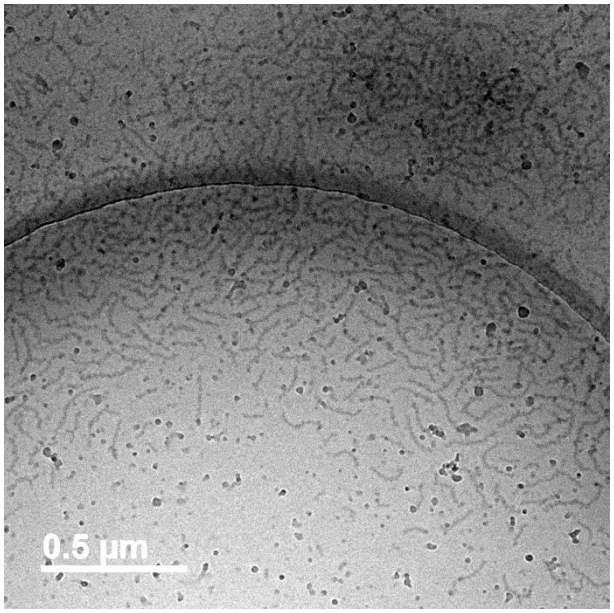

Figure SI 19 Cryo-TEM image of the sample PEG-*b*-P(*NBoc*Lys).

Table SI 1: Characteristics of the copolymers obtained by ROPISA and their corresponding nanoparticles.

Copolymer	Buffer	Initiator	[M]/[I]	M_n	τ_s (%)	[M]/[I]	M_n	M_n	$Đ$	M_n	$Đ$	D_h (σ)	Y
				g/mol			g/mol	g/mol		g/mol		nm	
			Theory			^{1}H NMR [a]		SEC, LS [b]		SEC, PS [c]		DLS [d]	
PEG_{5k}-NH_2	-	-	-	5000	-	-	-	4900	1.08	6996	1.02	-	
PEG-*b*-PBLG **1**	$NaHCO_3$ 50mM	PEG_{5k}-NH_2	19	9160	7	20 (22)	9380	9360	1.10	11940	1.05	79 (0.08)	
PEG-*b*-PBLG **2**	$NaHCO_3$ 50mM	PEG_{5k}-NH_2	19	9160	4	21 (21)	9600	8920	1.08	11710	1.04	83 (0.10)	
PEG-*b*-PBLG **3**	$NaHCO_3$ 50mM	PEG_{5k}-NH_2	19	9160	10	21 (23)	9600	9940	1.09	12070	1.06	80 (0.11)	
PEG-*b*-PBLG **4**	$NaHCO_3$ 50mM	PEG_{5k}-NH_2	19	9160	13	21 (24)	9600	9690	1.12	12250	1.06	88 (0.17)	
PEG-*b*-PBLG **5**	MQ	PEG_{5k}-NH_2	19	9160	7	20 (19)	9380	10550	1.36	13470	1.14	110 (0.13)	
PEG-*b*-PBLG **6**	$NaHCO_3$ 50mM	PEG_{5k}-NH_2	38	13320	10	35 (41)	12670	11250	1.16	14370	1.09	99 (0.12)	
PEG_{10k}-*b*-PBLG **7**	$NaHCO_3$ 50mM	PEG_{10k}-NH_2	38	18320	13	37 (47)	18100	18580	1.15	24660	1.12	gel	
PEG-*b*-(*NBoc*Plys)	$NaHCO_3$ 50mM	PEG_{5k}-NH_2	18	9100	7	21 (20)	9790	nd	nd	11750	1.09	131 (0.19)	
PBLG **1**	MQ	none	-	-	7	-	-	-	-	924	11.8	-	
PBLG **2**	$NaHCO_3$ 200mM	Ethanolamine	19	4220	3	-	-	-	-	1560	1.84	-	
PBLG **3**	$NaHCO_3$ 200mM	PEG_{5k}-OH	-	-	7	-	-	-	-	4520	2.86	-	

[a] Degree of polymerization (**[M]/[I]**) and number average molar mass (***M*$_n$**) determined by 1H NMR using the CH_2 of the mPEG-NH_2 as an internal reference (see methods). [M]/[I[in brackets are calculated using the CH_3 term of the mPEG-NH_2 as an internal reference. [b] Absolute number average molar mass (***M*$_n$**) and dispersity (***Đ***) determined by SEC using a multi-angle static light scattering detection [c] Number average molar mass (***M*$_n$**) and dispersity (***Đ***) determined by SEC in DMF (+LiBr) using a polystyrene calibration curve. [d] Hydrodynamic diameter (***D*$_h$**) and polydispersity (**σ**) determined using a Malvern apparatus.

C. Grazon, P. Salas-Ambrosio, E. Ibarboure, A. Buol, E. Garanger, M.W. Grinstaff, S. Lecommandoux, C. Bonduelle, Angewandte Chemie International Edition 2019. DOI 10.1002/anie.201912028